BSLJ (Building Standard Law of Japan). 2000. *Building standard law*. Buildings Center of Japan.

Davenport, A. G. 1967. "Gust loading factor." *J. Struct. Div.* **93**, 11–34.

Hokkoku Shimbun. 2007. "Morning issue." November 13, 2007.

National Standard of China. 2011. *Technical code for safety of steel tubular scaffold with couplers in construction*. Ministry of Housing and Rural-Urban Development of China.

Ohdo, K. 2007. *Wind engineering handbook*, edited by JAWE, Asakura-shoten, 232.

SCEAJ-TRSSW (Scaffolding and Construction Equipment Association of Japan–Technical Recommendation for Safety of Scaffolding to Winds). 1999. *Technical Recommendation for Safety of Scaffolding to Winds*. Scaffolding and Construction Equipment Association of Japan (Kasetsu Kogyo Kai).

Tamura, Y. 2009. "Wind and tall buildings." In *Proc., 5th European and African Conf. on Wind Engineering (EACWE 5)*, 25–49, Florence, Italy.

Tamura, Y., H. Niino, O. Suzuki, Y. Fujiyoshi, H. Kawai, and Y. Okuda. 2007. *Investigation of serious tornado damage in Saroma-cho*. Special Research Promotion Grant No. 18900003. Hokkaido, Japan: JSPS.

CHAPTER 6

Simulating the Role of Axial Flow in Stay Cable Vibrations via a Perforated Wake Splitter Plate

Ran Wang[*]
Shaohong Cheng[*]
David S-K. Ting[†]

Abstract: *The inclined and/or yawed orientation of bridge stay cables results in the formation of secondary axial flow on the leeward side of cable surface, which is believed to be one of the contributing factors exciting some unique wind-induced cable vibration phenomena. To clarify the role of axial flow in triggering aerodynamic instability of stay cables, a numerical study has been conducted to indirectly examine the axial flow effect via a perforated splitter plate placed along the central line of a circular cylinder wake. By manipulating the perforation ratio of the perforated plate at four different levels, the variation of von Kármán vortex shedding strength, which reflects the axial flow intensity, can be simulated. The impact of the splitter plate perforation ratio on the flow structure around a circular cylinder, in terms of the instantaneous vortex structure, the surface pressure distribution and the aerodynamic forces are discussed in detail by exploiting the numerical data obtained from the large eddy simulation. Results show that the presence of a perforated wake splitter plate would play a similar role as the axial flow in affecting the strength of von Kármán vortex shedding. A more solid wake splitter plate is found to cause a stronger interruption on the interaction between the shear layers formed on the two sides of the cylinder and consequently lead to a more symmetric surface pressure distribution pattern and weaker von Kármán vortex shedding strength. Reductions on the fluctuating amplitude of the instantaneous lift and drag as well as the mean drag are also observed, which would ultimately affect the aerodynamic response of the studied cylinder.*

[*]Department of Civil and Environmental Engineering, University of Windsor (corresponding author), Tel: +15192533000, Ext. 2629, Fax: +5199713686, email: {wang1hf, shaohong}@uwindsor.ca

[†]Department of Mechanical, Automotive and Materials Engineering, University of Windsor 401 Sunset Avenue, Windsor, Ontario, Canada, N9B 3P4, email: dting@uwindsor.ca

Keywords: *circular cylinder; perforated wake splitter plate; von Kármán vortex shedding; axial flow; cable vibrations; cable-stayed bridges; aerodynamic instability; large eddy simulation.*

1 INTRODUCTION

Cable-stayed bridges have become progressively popular since the completion of the Stromsund Bridge in Sweden in 1955, mainly due to their modest requirement on ground anchorage condition, efficient utilization of structural material, higher stiffness and economy compared to the suspension bridges. Rapid development in materials, design and construction technology constantly push the bridge span to a new limit. Currently, the record holder of the cable-stayed bridge, the Russky Bridge in Russia, has a center span length of 1,104 m and the longest cable on the bridge is 580 m. The road deck of the highest cable-stayed bridge, the Duge Bridge in China inaugurated in 2016, sits over 565 m above the Beipan River. These great advancements are, naturally, accompanied with new engineering challenges. Owing to the low lateral stiffness, low inherent damping and small mass, stay cables on cable-stayed bridges are prone to dynamic excitations. Further, the inclined and/or yawed orientation of stay cables against the oncoming wind introduces some unique wind-induced cable vibration phenomena, the mechanisms of which are yet to be fully comprehended.

Excessive vibrations of cables on cable-stayed bridges have been frequently reported in recent years. Among these incidents, rain-wind-induced vibration (RWIV) is observed most on site. This sort of vibration was first reported by Hikami and Shiraishi (1988) on the Meiko-Nishi Bridge in Japan. After that, numerous similar cases were reported (Stafford and Watson 1988, Pacheco 1993, Persoon and Noorlander 1999, Main and Jones 2000, Matsumoto et al. 2003, Zuo et al. 2008, Zuo and Jones 2010). Extensive researches have been conducted to unveil the mystery, mainly using wind tunnel tests (Matsumoto et al. 1992, 1995; Flamand 1995; Bosdogianni and Olivari 1996; Ming 2002; Gu and Du 2005; Alam and Zhou 2007; Li et al. 2016; Jing et al. 2017), theoretical (Yamaguchi 1990; Gu and Lu 2001; Cao et al. 2003; He et al. 2010, 2012; Li et al. 2013) and numerical analyses (Seidel and Dinkler 2006, Robertson et al. 2010, Li et al. 2010, Bi et al. 2013, Wang et al. 2016). While many studies have been carried out to investigate the excitation mechanisms of RWIVs, researchers held different or even conflicting ideas and no consensus has been reached so far (Jing et al. 2017b). Nevertheless, the formation of upper water rivulet on the cable surface is considered to be an important factor to induce RWIV.

Dry inclined cable galloping has been proved theoretically to be a potential safety threat to bridge stay cables (Piccardo 1993, Macdonald and Larose 2008, Raeesi et al. 2014, He and Macdonald 2016). Saito et al. (1994) proposed an instability criterion which suggested that the onset condition of dry inclined cable galloping could be easily satisfied for many stay cables on existing bridges and the unstable cable motion could not be suppressed by introducing additional damping. However, this criterion is too conservative to be applied to bridge design and field experience indicated that this was not the case. Outcomes of earlier studies indicated that the necessary conditions to trigger dry inclined cable galloping would include (a) emergence of critical Reynolds number regime (Macdonald and Larose 2006; Cheng et al. 2008a, 2008b), (b) presence of axial flow (Matsumoto et al. 1992, 1995, 2003, 2005), and (c) sustained duration of the critical flow condition (Raeesi et al. 2014). Also, high span-wise correlation of aerodynamic forces on the cable upon the onset of dry galloping was found by Cheng and Tanaka (2005). It is worth noting that, up till now, no field incident of dry inclined cable galloping has been formally confirmed, despite a few wind tunnel tests (Miyata et al. 1994; Cheng et al. 2003, 2008b; Jakobsen et al. 2012; Vo et al. 2016) observed the occurrence of this type of instability. reported both divergent and limited-amplitude cable vibrations at high reduced wind speed. Zuo and Jones (2009) suspected that the dry galloping observed in the wind tunnel test by Cheng et al. (2003, 2008a) might relate to rain-wind-induced vibration in the field. However, it is challenging in acquiring accurate onsite environment data at the occurrence of violent cable vibrations, such as the particular amount of precipitation, wind speed and direction. The possible existence of the so-called rain-wind-induced vibration in the absence of rainfall, and the possible relation between the vibrations observed on wet and dry cables is still unclear.

A circular cylinder in cross-flow has been extensively studied both experimentally and numerically. However, in the case of a bridge stay cable, though it is typically modeled as a circular cylinder in existing studies, the flow structure around it is much more complex due to its inclined and yawed orientation. This renders the formation of the secondary axial flow on the leeward side of the cable surface which disturbs the interaction between the shear layers separated from the two sides of the cylinder and suppresses the shedding of the von Kármán vortices. Shirakashi et al. (1986) investigated the aerodynamic behaviour of a yawed circular cylinder in uniform flow in the wind tunnel and concluded that the reduction of the vortex shedding frequency by yawing was attributed to the presence of the secondary flow behind the cylinder. Matsumoto et al. (1990) reported that depending on the boundary condition, the intensity of the axial flow formed on the leeward side of a circular cylinder yawed at 45° varied between 40% to 60% of the oncoming flow velocity.

From the existing studies, it is understood that a splitter plate could be used as a passive device to control the vortex formation in the wake of a cylinder (Roshko and Anato 1954, Apelt et al. 1973, Apelt and West 1975, Ozono 1999, Choi 2007, Dehkordi and Jafari 2010, Ali et al. 2012). Therefore, it is expected that a wake splitter plate would play a similar role as that of the axial flow in interrupting the communications between separated flow from the two sides of a cylinder. Due to the challenge of directly manipulating and measuring the intensity of axial flow, Matsumoto et al. (2010) installed a perforated splitter plate in the wake center of a non-yawed circular cylinder in a wind tunnel study. By varying the perforation ratio of the splitter plate, the intensity of von Kármán vortex shedding from the cylinder body can be controlled in a stationary state. Their results implied that the generation mechanism of dry inclined cable galloping might be associated with the suppression of the von Kármán vortex shedding.

Many researchers investigated the impact of placing a solid plate in the near wake of a cylinder on its surrounding flow structure. (Roshkot 1954) discovered that the base pressure of a circular cylinder would be substantially increased if a long solid splitter plate was present in the wake. Apelt et al. (1973) and Apelt and West (1975) conducted experiments by placing solid splitter plate of different lengths downstream of a circular cylinder. They concluded that the near wake structure of the cylinder might be studied in the absence of von Kármán vortex formation. A few other studies also discussed how the communication interruption between the separated shear layers in the wake region of a cylindrical body in the presence of a solid splitter plate would affect the aerodynamic forces acting on it (Ozono 1999, Choi 2007, Dehkordi and Jafari 2010, Ali et al. 2012). On the other hand, experimental studies on the effect of a perforated/permeable wake splitter plate on the flow structure around a circular cylinder were rarely reported in literature. Cardell (1993) indicated that if a permeable splitter plate was placed in the wake of a cirucluar cylinder, both drag and von Kármán vortex shedding frequency would drop. In addition, provided the plate solidity was high enough, the base pressure of the cylinder was found to be independent of the Reynolds number and the plate solidity. As far as the numerical simulation is concerned, the solid wake splitter plate effect was investigated by a number of researchers in the relatively low Reynolds number regime (Kwon and Choi 1996; Hwang et al. 2003, 2007; Vu et al. 2015); whereas to the best knowledge of the authors, reported numerical study on the flow structure around a circular cylinder with a perforated wake splitter plate is scarce.

Existing studies showed that the extent of communication between the separated shear layers was critical to the characteristics of the cylinder wake. Abernathy and Kronauer (1962) proposed that, in the subcritical Reynolds number region, the von Kármán vortex street could form without a wake producing body, but rather by just bringing two shear layers of opposite sign within a communicable proximity of one another. Cardell (1993) confirmed the ability of permeable splitter plate in modifying the communication across the center plane of a circular cylinder wake. The effect of axial flow, on the other hand, on interrupting the communication between the two separated shear layers in the near wake region behind a circular cylinder was reported by Matsumoto et al. (2010). It was also suspected that the formation of axial vortex on the leeward side of the cylinder and the possible interaction between the axial vortex shedding and the conventional von Kármán vortex shedding in the wake could contribute to the aerodynamic instability of the cylinder. Their results indicated that galloping could be excited by introducing artificial axial flow in the near wake of a non-yawed circular cylinder. However, quite counter intuitively, it was also found that the velocity of axial flow, which might be related to the degree of interference on shear layer communication, had an inverse relation with the stability of the circular cylinder. Though the mechanism of axial flow on affecting the aerodynamic stability of a circular cylinder has not been fully unveiled, it is clear that part of its role is similar as that of the splitter plate, i.e. to interrupt the shear layer communication. Therefore, it is feasible to apprehend our understanding of the effect of axial flow, as well as its intensity, on the aerodynamic stability of a circular cylinder via placing a splitter plate with variable perforation ratio in its wake.

To unveil the possible relation between the von Kármán vortex shedding mitigation and the onset of dry inclined cable galloping, it is imperative to examine how change in the communication of separated shear layers would influence the flow structure around a circular cylinder and/or vice versa. In the current paper, a CFD simulation will be conducted to study flow past a non-yawed circular cylinder at a Reynolds number of 3900, with the presence of a perforated wake splitter plate. This particular Reynolds number is selected mainly due to the availability of the existing experimental and numerical data, which can be used to validate the developed numerical model. By manipulating the solidity of the perforated wake splitter plate, the variation of von Kármán vortex shedding strength can be simulated. This would allow examining the impact of axial flow intensity on the aerodynamic behaviour of a circular cylinder indirectly and shed light on the role of axial flow in the excitation mechanism of dry inclined cable galloping.

2 NUMERICAL SIMULATION

2.1 Numerical approach

All simulations presented in this paper utilize the open source CFD Toolbox: OpenFOAM V4.1 (Open Source Field Operation and Manipulation). The incompressible solver pisoFOAM uses a finite volume cell-centered discretization of the domain and handles unstructured mesh data format based on the so-called face-addressing storage using Pressure-Implicit with Splitting of Operators algorithm (PISO). Linear Green-Gauss is used for computing the gradient. The treatments of convective terms for velocity, kinematic turbulent energy, kinematic turbulent viscosity are Gauss LUST (blended 75% linear and 25% linearUpwind) and Gauss limitedLinear for the last two terms. A second-order accuracy scheme backward method is used for temporal discretization. A time step of 10^{-4} second is employed to guarantee the maximum Courant number to be smaller than 0.2 during the simulation. A geometric agglomerated algebraic multigrid solver (GAMG) with the Gauss-Seidel smooth method iteratively solves the linear algebraic system with a local accuracy of 10^{-6} for the pressure and 10^{-7} for the remaining variables at each time step.

The current study mainly focuses on the unsteady-state flow and hence the detailed instantaneous flow characteristics are critical to the investigation. In the Reynolds-averaged Navier-Stokes (RANS) approach, one only solves the averaged fluid field while the effect of all scales of instantaneous turbulent motion is modelled by a turbulent model. The direct numerical simulation (DNS) directly solves the full Navier-Stokes equations using extremely fine spatial and temporal discretization to capture eddies at all scales in the given problems at a huge computational cost. The large eddy simulation (LES) is based on the filtered Navier-Stokes equations (Smagorinsky 1963). Instead of adopting the conventional time averaging RANS approach with additional modelled transport equations, LES simulates eddies which are larger than the smallest grid size directly, while it treats the eddies under this scale by using the subgrid-scale (SGS) model with relatively lower computational resources than DNS. A novel approach of the hybrid LES-RANS method, i.e. the detached eddy simulation (DES), solves the attached portion of the boundary layers with the traditional RANS and uses LES in the separated flow regions. However, when using DES, the treatment of the boundary layer in the vicinity of the cylinder is not sufficient to unveil the properties of the highly unsteady flow. Therefore, the LES turbulent model is adopted in the current study to investigate the effect of a perforated wake splitter plate on the flow characteristics around a circular cylinder.

The governing equations, the Navier-Stokes equations, are based on the conservation laws for mass, momentum and energy. Since only the large eddies are directly computed in LES, so a low-pass spatial filter is applied to the Navier-Stokes equations. The filtered equations for a Newtonian incompressible flow can be written in a conservative form as

$$\partial_i \overline{u}_i = 0 \tag{1}$$

$$\partial_t(\rho \overline{u}_i) + \partial_j(\rho \overline{u}_i \overline{u}_j) = -\partial_i \overline{p} + 2\partial_j(\mu \overline{S_{ij}}) - \partial_j(\tau_{ij}) \tag{2}$$

$$\overline{S_{ij}} = \frac{1}{2}(\partial_i \overline{u}_j + \partial_j \overline{u}_i) \tag{3}$$

$$\tau_{ij} = \frac{1}{2}(\overline{u_i u_j} - \overline{u}_i \overline{u}_j) \tag{4}$$

where ρ is the density of the air, $\overline{u}_i$ is the filtered velocity, $\overline{p}$ is the filtered pressure, μ is the dynamics viscosity, $\overline{S_{ij}}$ is the filtered strain rate tensor, and τ_{ij} is the unknown SGS stress tensor, which represents the small scale motions. To solve the above equations, the SGS eddy viscosity needs to be determined. The most basic model is the one originally proposed by Smagorinsky (1963):

$$\mu_t = \rho(C_s \overline{\Delta})^2 S \tag{5}$$

$$S = (2\overline{S}_{ij}\overline{S}_{ij})^{\frac{1}{2}} \tag{6}$$

$$\Delta = (\Delta x \Delta y \Delta z)^{\frac{1}{3}} \tag{7}$$

where C_s is the Smagorinsky constant depending on the type of the flow.

2.2 Computational domain

The coordinate system, the definition of the angle θ, which represents the angular position of an arbitrary point on the cylinder surface with respect to the stagnation point, and the span-wise length are shown in the Figure 1a. Figure 1b illustrates a schematic view of the computational domain of a classic case of flow past a circular cylinder. The diameter of the studied circular cylinder is $D = 0.0889$ m. The center of the cylinder coincides with the origin of the computational domain. From the origin, the computational domain extends $10D$ toward the inlet and $20D$ toward the outlet, and from -$10D$ to $10D$ in the cross-flow direction. The span-wise extension L_z is chosen to be $\pi D/2$, which is found to be more efficient while maintaining an acceptable accuracy based on the mesh independence test.

ANSYS/ICEM is used to generate a block structured rectangular computational domain, as shown in Figure 1b. The non-dimensional viscous length scale is defined as

$$y^+ = (u_* \cdot y)/\nu \tag{8}$$

where u_* is the friction velocity at the near wall, y is the distance to the wall and ν is the local kinematic viscosity of the fluid. The height of the first cell on the cylinder is $9.57 \times 10^{-4}D$, which guarantees y^+ is smaller than 1. The no-slip condition is imposed on the surface of the cylinder and the plate. The span-wise resolution Δz is $0.05D$ with 32 nodes along the z-axis. 392 nodes are employed on the cylinder surface along the circumference for the no wake splitter plate case. The total number of control volumes for the solid plate case is 5.57×10^6. A non-dimensional time step Δt of 7.4×10^{-4} is used, where $\Delta t = Ut/D$. A Dirichlet boundary condition for velocity $(u = 0.658\,m/s; v = 0; w = 0)$ and a Neumann boundary condition for zero gradient pressure are prescribed at the inlet. A Dirichlet boundary condition for zero pressure is applied at the outlet. A cyclic boundary condition is employed on the span-wise walls.

When introducing a piece of splitter plate along the central line of a circular cylinder wake, not only the perforation ratio, but also the size and the position

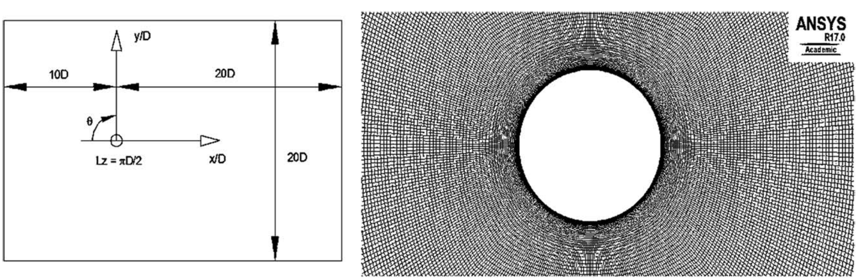

(a) (b)

Figure 1. Computational domain and detailed mesh for flow past a circular cylinder: (a) computational domain, and (b) detailed grid in the near region of the circular cylinder

of the plate could have a sizable impact on the cylinder wake structure. (Roshkot 1954) found that a splitter plate of length 5*D* (*D* is the cylinder diameter) inhibited the periodic formation of the von Kármán vortices, whereas it was not the case if the plate length was shortened to 1.14*D*. Besides, Cardell (1993) investigated the influence of the gap size between the splitter plate and the cylinder on the flow properties around the cylinder. Results showed that if the gap was less than 0.13*D*, the presence of the splitter plate would not have an appreciable effect on the cylinder mean base pressure and the von Kármán vortex shedding frequency. Based on these, to explore how the variation of the von Kármán vortex shedding strength would affect the flow structure around a circular cylinder, in the current numerical study, a wake splitter plate of length *D* and thickness *D*/20 was placed along the central line of the cylinder wake with a gap of 0.11*D* between the cylinder and the plate.

Figure 2 shows a 3D view of the detailed mesh near the cylinder and the solid wake splitter plate. For the perforated plate, the perforation ratio is defined as the ratio between the opening length and the total length of the splitter plate along the flow direction. A total of four perforation ratio levels, i.e. 0, 1/3, 2/3, and 1, are simulated in the current study, of which a perforation ratio of 0 represents the solid splitter plate case, whereas 1 represents the no splitter plate case. The mesh details of the perforation ratio cases of 1/3 and 2/3 are given in Figures 3a and 3b, respectively.

Regarding the mesh generation scheme in the perforated splitter plate cases, the O-shape meshes were first introduced in the near region of the cylinder. Then, based on the studied perforation ratio, the block near the splitter plate region was further divided into 7 and 16 sub-blocks, with the quadrilateral meshes generated in each sub-block. Finally, the three-dimensional meshes were generated by extending the two-dimensional plane along the span-wise direction.

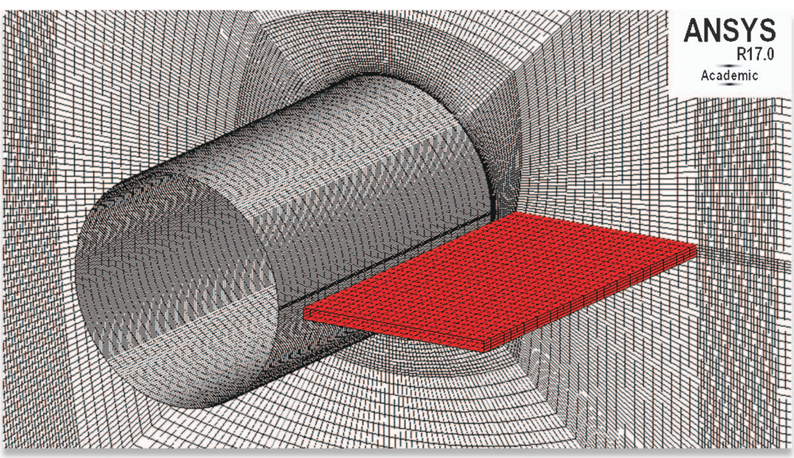

Figure 2. Detailed mesh near the cylinder and the solid splitter plate (perforation ratio of 0)

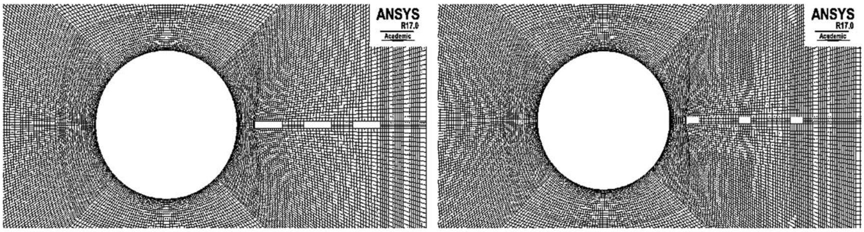

Figure 3. Mesh details of the perforated wake splitter plate cases: (a) perforation ratio of 1/3, and (b) perforation ratio of 2/3

2.3 Model validation

The validity of the developed numerical model was examined using the no splitter plate case at a Reynolds number of 3900. Two different meshes, Mesh 1 and Mesh 2 were used for the model validation test. They had the same 2-dimensional grid, but the number of nodes in the span-wise direction was taken as 16 and 32, respectively. The span-wise resolution (i.e., the distance between the two adjacent span-wise nodes) was kept the same at $\pi D/64$. The drag coefficient and the Strouhal number of the circular cylinder obtained from these two meshes are listed in Table 1, along with the data reported in literature (Lourenco and Shih 1993, Breuer 1998, Kravchenko and Moin 2000, Tremblay

Table 1. Model Validation Results

Model	*Method*	*Number of vortex shedding periods*	*Number of control volume (million)*	C_d	S_t
Mesh 1	LES	10	2.3	1.32	0.22
Mesh 2	LES	10	5.5	1.20	0.21
Lourenco and Shih (1993)	PIV	–	–	0.99	0.22
Breuer (1998)	LES	22	0.87 to 1.74	[0.97–1.49]	[0.21–0.22]
Kravchenko and Moin (2000)	LES	7	0.5 to 2.4	[1.04–1.36]	[0.19–0.21]
Tremblay et al. (2002)	LES	–	–	[1.14–1.31]	[0.21–0.22]
Prsic et al. (2012)	LES	60	5 to 11	[1.10–1.24]	0.21